Geophysical Research Letters

Supporting Information for

Re-evaluating the contribution of sulfuric acid and the origin of organic compounds in atmospheric nanoparticle growth

Ville Vakkari[1], Petri Tiitta[2,3], Kerneels Jaars[2], Philip Croteau[4], Johan Paul Beukes[2], Miroslav Josipovic[2], Veli-Matti Kerminen[5], Markku Kulmala[5], Andrew D. Venter[2], Pieter G. van Zyl[2], Douglas R. Worsnop[4,5], and Lauri Laakso[1,2]

[1]Finnish Meteorological Institute, Research and Development, FI-00101 Helsinki, Finland.

[2]North-West University, Unit for Environmental Sciences and Management, ZA-2520 Potchefstroom, South Africa.

[3]University of Eastern Finland, Department of Environmental Science, FI-70211 Kuopio, Finland.

[4]Center for Aerosol and Cloud Chemistry, Aerodyne Research, Inc., Billerica, MA, USA.

[5]University of Helsinki, Department of Physics, FI-00014 Helsinki, Finland.

Contents of this file

Text S1 to S2
Figures S1 to S8
Tables S1 to S3

Additional Supporting Information (Files uploaded separately)

Introduction

This file contains supplementary materials and methods including supplementary references, supplementary Figures S1 to S8 and supplementary Tables S1 to S3.

Text S1. Supplementary materials and methods

1. Connection between secondary aerosol formation and new-particle growth

During a new particle formation event the change in secondary aerosol mass in the submicron size range, as measured by the ACSM (Q_{ACSM}), can be written as

$$Q_{\mathrm{ACSM}} = Q_{\mathrm{OA}} + Q_{\mathrm{SO4}} + Q_{\mathrm{NH4}} + Q_{\mathrm{NO3}}, \quad \text{(S1)}$$

where the terms Q_i refer to the submicron mass change caused by changes in the measured OA, SO_4^{2-}, NH_4^+ and NO_3^- concentrations.

Here, we focus on periods with simultaneous new-particle growth and submicron aerosol mass increase. For such periods, we can determine the increases in Q_i (i= OA, SO_4^{2-}, NH_4^+ or NO_3^-), and thereby Q_{ACSM}, from linear fits to the ACSM data (see Fig. S4). Such a fit was also made for Cl^-; however, this compound never gave important contribution to Q_{ACSM}, so it was omitted from further discussion. The NPF event period for the fit was identified using measured particle size distributions. Similar methods have been used by e.g. Zhang et al. [2011b] and Setyan et al. [2014].

In addition to chemical partitioning, observed changes in Q_{ACSM} may also be partitioned between different aerosol dynamical and atmospheric processes:

$$Q_{\mathrm{ACSM}} = Q_{\mathrm{COND,KIN}} + Q_{\mathrm{COND,SV}} + Q_{\mathrm{HET}} + Q_{\mathrm{TRANS}}, \quad \text{(S2)}$$

Here, the sum of $Q_{\mathrm{COND,KIN}}$ and $Q_{\mathrm{COND,SV}}$ is the total submicron aerosol mass increase due to vapor condensation from the gas phase, Q_{HET} represents the mass increase through heterogeneous formation pathways [*Pöschl*, 2011], and Q_{TRANS} represents changes in the submicron aerosol mass caused by air mass transport effects. Of the two vapor condensation terms, $Q_{\mathrm{COND,KIN}}$ is for the subset of vapors capable of growing <30 nm diameter particles, i.e. essentially low and extremely low-volatile vapors [*Donahue et al.*, 2011, 2012; *Ehn et al.*, 2014], while $Q_{\mathrm{COND,SV}}$ accounts for the rest of condensable vapors, i.e. essentially intermediate volatile and semi-volatile vapors [*Donahue et al.*, 2011, 2012].

The term Q_{TRANS} may become important due to dilution of polluted boundary-layer air, entrainment of pollution into a clean boundary layer, or due to rapid changes in the character of measured air masses. In order to minimize the effects of Q_{TRANS} and potential other problems with the data, we estimated Q_{ACSM} only for those periods when no abrupt changes in the background aerosol population occurred. Furthermore, Q_{ACSM} was estimated only when the submicron aerosol mass (PM_1) obtained from the ACSM and derived from the DMPS agreed to within 20 % of each other.

The gas-phase concentration, C, of the vapors responsible for $Q_{\mathrm{COND,KIN}}$ is determined by the following balance equation:

$$\frac{dC}{dt} = P - \mathrm{CS} \times C - Q_{\mathrm{J12}}, \quad \text{(S3)}$$

where P is the gas-phase production rate of these vapors, CS is the condensation sink that particles larger than 12 nm in diameter represent for these vapors [*Kulmala et al.*, 2012], and Q_{J12} is the sink that the formation of 12 nm particles represents to these vapors. We estimated Q_{J12} from the relation

$$Q_{J12} = J12 \times \frac{4\pi}{3} \times R^3 \times \rho, \quad \text{(S4)}$$

where R=8.7 nm, i.e. the geometric mean radius of the size range used to calculate J_{12}, and ρ=1.83 g cm^{-3}.

By assuming a pseudo-steady state for the vapors responsible for $Q_{\mathrm{COND,KIN}}$ (dC/dt ≈0), we obtain:

$$P \approx Q_{\mathrm{COND,KIN}} \approx \mathrm{CS} \times C + Q_{\mathrm{J12}} \quad \text{(S5)}$$

The observed particle growth rate of 12−30 nm particles, GR, is directly proportional to the gas-phase concentration C [*Kulmala et al.*, 2012]:

$$C = A\left(\mathrm{GR} - \mathrm{GR}_o\right) \quad \text{(S6)}$$

Here, GR_o presents new-particle growth by processes other than vapor condensation, and A is a factor that depends on the properties of condensing vapor and particles size. We determined A separately for each GR range according to Nieminen et al. [2010] assuming molecular properties of sulfuric acid for condensing vapors (see Table S2).

Next, we define the quantity Q_{GR} by following Kulmala et al. [2012]:

$$Q_{GR} = CS \times A \times GR \quad \text{(S7)}$$

By combining equations S2, S5, S6 and S7, we finally obtain:

$$Q_{\mathrm{ACSM}} = Q_{\mathrm{GR}} + Q_{J12} + Q_{\mathrm{COND,SV}} + Q_{\mathrm{HET}} + Q_{\mathrm{TRANS}} - CS \times A \times GR_o \quad \text{(S8)}$$

The sum Q_{GR} + Q_{J12} is the total condensable vapor source rate required to produce the observed values of GR and J_{12} simultaneously. On average (median), Q_{J12} was 9 % of $Q_{\mathrm{GR12\text{-}30}}$ in our data set.

2. Estimating sulfuric acid concentration

Gas phase sulfuric acid (H_2SO_4) concentration was estimated with a proxy calculated according to equation 9 in Mikkonen et al. [2011]. The proxy is based on observed sulfur dioxide (SO_2) concentration, CS, global radiation, temperature (T) and relative humidity (RH). At Welgegund SO_2 was measured with a Thermo 43S gas analyser, global radiation was measured with a Kipp&Zonen CMP-3 and T and RH with a Rotronic MP101A [*Petäjä et al.*, 2013].The constant coefficients in the proxy have been determined from a least squares fit to chemical ionization mass spectrometry (CIMS) [e.g. *Eisele and Tanner*, 1993; *Berresheim et al.*, 2000] measurements during six field campaigns [*Mikkonen et al.*, 2011].

The estimated H_2SO_4 concentration ($C_{\mathrm{H2SO4,proxy}}$) can be used to estimate the GR due to H_2SO_4, ($\mathrm{GR}_{\mathrm{calc}}$) from equation S6 assuming that $\mathrm{GR}_o \approx 0$:

$$GR_{calc} = \frac{C_{H2SO4,proxy}}{A} \quad \text{(S9)}$$

Alternatively, the GR due to H_2SO_4 can be estimated from the observed $\mathrm{GR}_{12\text{-}30}$ from the size distribution measurements and the observed fraction of Q_{SO4} of the total Q_{ACSM}, similar to e.g. Bzdek et al. [2012]. We denote this estimate of GR due to H_2SO_4 as $\mathrm{GR}_{\mathrm{SO4}}$,

$$GR_{SO4} = \frac{Q_{SO4}}{Q_{ACSM}} \cdot GR_{12-30} \quad \text{(S10)}$$

Additionally, we have estimated the total gaseous sulfuric acid concentration (Fig. 4b) from the observed GR, CS, Q_{ACSM} and Q_{SO4} as

$$C_{H2SO4,tot} = \frac{Q_{SO4}}{Q_{ACSM}} \times Q_{GR} \quad . \qquad \text{(S11)}$$

3. Air mass history

Air mass history was studied by calculating hourly 96-hour back-trajectories with the HYbrid Single-Particle Lagrangian Integrated Trajectory (HYSPLIT) version 4.8 model [*Draxler and Hess*, 1998]. As meteorological input data we used GDAS archive produced by the US National Weather Service's National Centre for Environmental Prediction (NCEP) and archived by National Oceanic and Atmospheric Administration (NOAA) Air Resources Laboratory (http://www.arl.noaa.gov/archives.php). The arrival height of the back-trajectories was 100 m above ground.

A NPF event was considered to represent the clean sector (cf. Fig. 3) if the back-trajectories for that time period spent on average (mean) at least 20 hours over the clean sector, less than four hours over the regional background sector north-east of Welgegund and completely avoided the industrialized Highveld region around Johannesburg. Similar criteria based on the time spent over each source region were applied to retrieve representative samples of NPF events from each region. The criteria are summarized in Table S3.

Text S2. Supplementary references

Ahlm, L. et al. (2012), Formation and growth of ultrafine particles from secondary sources in Bakersfield, California, *J. Geophys. Res. Atmos.*, *117*(D21), D00V08, doi:10.1029/2011JD017144.

Allan, J. D. et al. (2006), Size and composition measurements of background aerosol and new particle growth in a Finnish forest during QUEST 2 using an Aerodyne Aerosol Mass Spectrometer, *Atmos. Chem. Phys.*, *6*(2), 315–327, doi:10.5194/acp-6-315-2006.

Berresheim, H., T. Elste, C. Plass-Dülmer, F. . Eiseleb, and D. . Tannerb (2000), Chemical ionization mass spectrometer for long-term measurements of atmospheric OH and H2SO4, *Int. J. Mass. Spectrom.*, *202*(1–3), 91–109, doi:10.1016/S1387-3806(00)00233-5.

Bzdek, B. R., C. A. Zordan, M. R. Pennington, G. W. Luther, and M. V. Johnston (2012), Quantitative Assessment of the Sulfuric Acid Contribution to New Particle Growth, *Environ. Sci. Technol.*, *46*(8), 4365–4373, doi:10.1021/es204556c.

Bzdek, B. R., A. J. Horan, M. R. Pennington, J. W. DePalma, J. Zhao, C. N. Jen, D. R. Hanson, J. N. Smith, P. H. McMurry, and M. V. Johnston (2013), Quantitative and time-resolved nanoparticle composition measurements during new particle formation, *Faraday Discuss.*, *165*(0), 25–43, doi:10.1039/C3FD00039G.

Bzdek, B. R., M. J. Lawler, A. J. Horan, M. R. Pennington, J. W. DePalma, J. Zhao, J. N. Smith, and M. V. Johnston (2014), Molecular constraints on particle growth during new particle formation, *Geophys. Res. Lett.*, *41*(16), 2014GL060160, doi:10.1002/2014GL060160.

Crilley, L. R., E. R. Jayaratne, G. A. Ayoko, B. Miljevic, Z. Ristovski, and L. Morawska (2014), Observations on the Formation, Growth and Chemical Composition of Aerosols in an Urban Environment, *Environ. Sci. Technol.*, *48*(12), 6588–6596, doi:10.1021/es5019509.

Donahue, N. M., E. R. Trump, J. R. Pierce, and I. Riipinen (2011), Theoretical constraints on pure vapor-pressure driven condensation of organics to ultrafine particles, *Geophys. Res. Lett.*, *38*(16), L16801, doi:10.1029/2011GL048115.

Donahue, N. M., J. H. Kroll, S. N. Pandis, and A. L. Robinson (2012), A two-dimensional volatility basis set – Part 2: Diagnostics of organic-aerosol evolution, *Atmos. Chem. Phys.*, *12*(2), 615–634, doi:10.5194/acp-12-615-2012.

Draxler, R., and G. Hess (1998), An overview of the HYSPLIT_4 modelling system for trajectories, dispersion and deposition, *Aust. Meteorol. Mag.*, *47*(4), 295–308.

Ehn, M. et al. (2014), A large source of low-volatility secondary organic aerosol, *Nature*, *506*(7489), 476–479.

Eisele, F. L., and D. J. Tanner (1993), Measurement of the gas phase concentration of H2SO4 and methane sulfonic acid and estimates of H2SO4 production and loss in the atmosphere, *J. Geophys. Res. Atmos.*, *98*(D5), 9001–9010, doi:10.1029/93JD00031.

Han, Y., Y. Iwamoto, T. Nakayama, K. Kawamura, and M. Mochida (2014), Formation and evolution of biogenic secondary organic aerosol over a forest site in Japan, *J. Geophys. Res. Atmos.*, *119*(1), 2013JD020390, doi:10.1002/2013JD020390.

Kulmala, M. et al. (2012), Measurement of the nucleation of atmospheric aerosol particles, *Nat. Protocols*, *7*(9), 1651–1667, doi:10.1038/nprot.2012.091.

Laakso, L. et al. (2008), Basic characteristics of atmospheric particles, trace gases and meteorology in a relatively clean Southern African Savannah environment, *Atmos. Chem. Phys.*, *8*(16), 4823–4839.

Mikkonen, S. et al. (2011), A statistical proxy for sulphuric acid concentration, *Atmos. Chem. Phys.*, *11*(21), 11319–11334, doi:10.5194/acp-11-11319-2011.

Nieminen, T., K. E. J. Lehtinen, and M. Kulmala (2010), Sub-10 nm particle growth by vapor condensation - effects of vapor molecule size and particle thermal speed, *Atmos. Chem. Phys.*, *10*(20), 9773–9779, doi:10.5194/acp-10-9773-2010.

Petäjä, T. et al. (2013), Transportable Aerosol Characterization Trailer with Trace Gas Chemistry: Design, Instruments and Verification, *Aerosol Air Qual. Res.*, *13*(2), 421–435, doi:10.4209/aaqr.2012.08.0207.

Pierce, J. R., I. Riipinen, M. Kulmala, M. Ehn, T. Petäjä, H. Junninen, D. R. Worsnop, and N. M. Donahue (2011), Quantification of the volatility of secondary organic compounds in ultrafine

particles during nucleation events, *Atmos. Chem. Phys.*, *11*(17), 9019–9036, doi:10.5194/acp-11-9019-2011.
Pierce, J. R. et al. (2012), Nucleation and condensational growth to CCN sizes during a sustained pristine biogenic SOA event in a forested mountain valley, *Atmos. Chem. Phys.*, *12*(7), 3147–3163, doi:10.5194/acp-12-3147-2012.
Pöschl, U. (2011), Gas–particle interactions of tropospheric aerosols: Kinetic and thermodynamic perspectives of multiphase chemical reactions, amorphous organic substances, and the activation of cloud condensation nuclei, *Atmos. Res.*, *101*(3), 562–573, doi:10.1016/j.atmosres.2010.12.018.
Riipinen, I., T. Yli-Juuti, J. R. Pierce, T. Petaja, D. R. Worsnop, M. Kulmala, and N. M. Donahue (2012), The contribution of organics to atmospheric nanoparticle growth, *Nature Geosci.*, *5*(7), 453–458, doi:10.1038/ngeo1499.
Setyan, A., C. Song, M. Merkel, W. B. Knighton, T. B. Onasch, M. R. Canagaratna, D. R. Worsnop, A. Wiedensohler, J. E. Shilling, and Q. Zhang (2014), Chemistry of new particle growth in mixed urban and biogenic emissions – insights from CARES, *Atmos. Chem. Phys.*, *14*(13), 6477–6494, doi:10.5194/acp-14-6477-2014.
Smith, J. N., M. J. Dunn, T. M. VanReken, K. Iida, M. R. Stolzenburg, P. H. McMurry, and L. G. Huey (2008), Chemical composition of atmospheric nanoparticles formed from nucleation in Tecamac, Mexico: Evidence for an important role for organic species in nanoparticle growth, *Geophys. Res. Lett.*, *35*(4), L04808, doi:10.1029/2007GL032523.
Vakkari, V., H. Laakso, M. Kulmala, A. Laaksonen, D. Mabaso, M. Molefe, N. Kgabi, and L. Laakso (2011), New particle formation events in semi-clean South African savannah, *Atmos. Chem. Phys.*, *11*(7), 3333–3346, doi:10.5194/acp-11-3333-2011.
Wiedensohler, A. et al. (2009), Rapid aerosol particle growth and increase of cloud condensation nucleus activity by secondary aerosol formation and condensation: A case study for regional air pollution in northeastern China, *J. Geophys. Res. Atmos.*, *114*(D2), D00G08, doi:10.1029/2008JD010884.
Zhang, Q., C. O. Stanier, M. R. Canagaratna, J. T. Jayne, D. R. Worsnop, S. N. Pandis, and J. L. Jimenez (2004), Insights into the chemistry of new particle formation and growth events in Pittsburgh based on aerosol mass spectrometry, *Environ. Sci. Technol.*, *38*(18), 4797–4809, doi:10.1021/es035417u.
Zhang, Y. M., X. Y. Zhang, J. Y. Sun, W. L. Lin, S. L. Gong, X. J. Shen, and S. Yang (2011), Characterization of new particle and secondary aerosol formation during summertime in Beijing, China, *Tellus B*, *63*(3), 382–394, doi:10.1111/j.1600-0889.2011.00533.x.

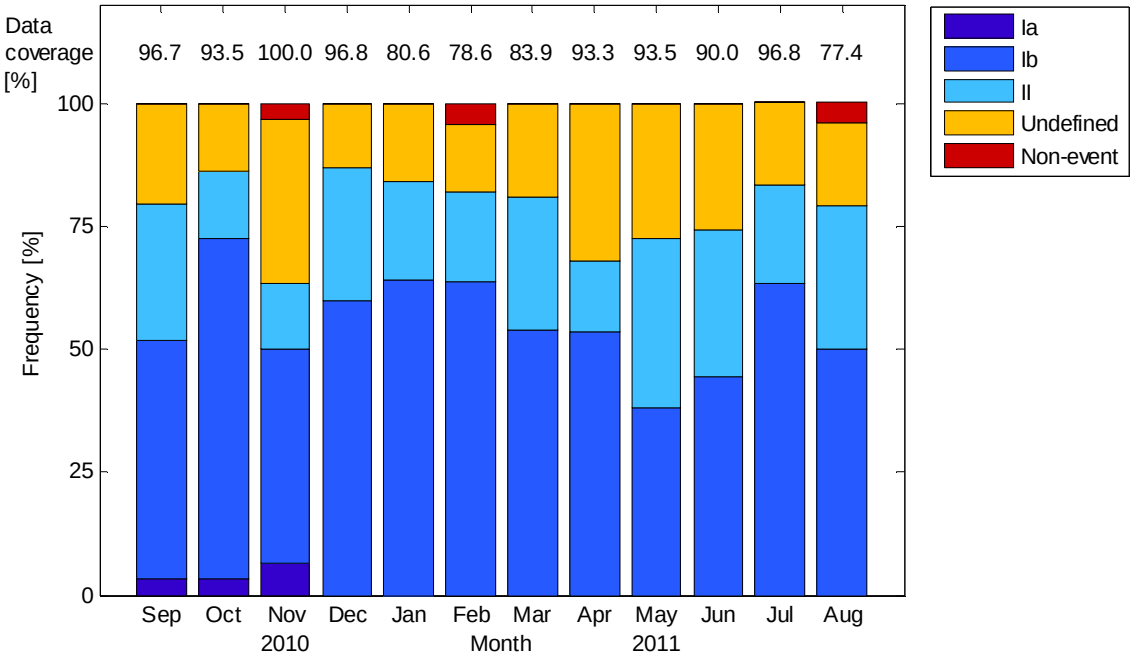

Figure S1. Seasonal variation of new particle formation frequency divided into five different classes [*Kulmala et al.*, 2012] based on DMPS measurements. NPF event classes Ia, Ib and II show clear, regional-scale formation of new particles and their subsequent growth [*Kulmala et al.*, 2012]. Also data coverage is shown for each month.

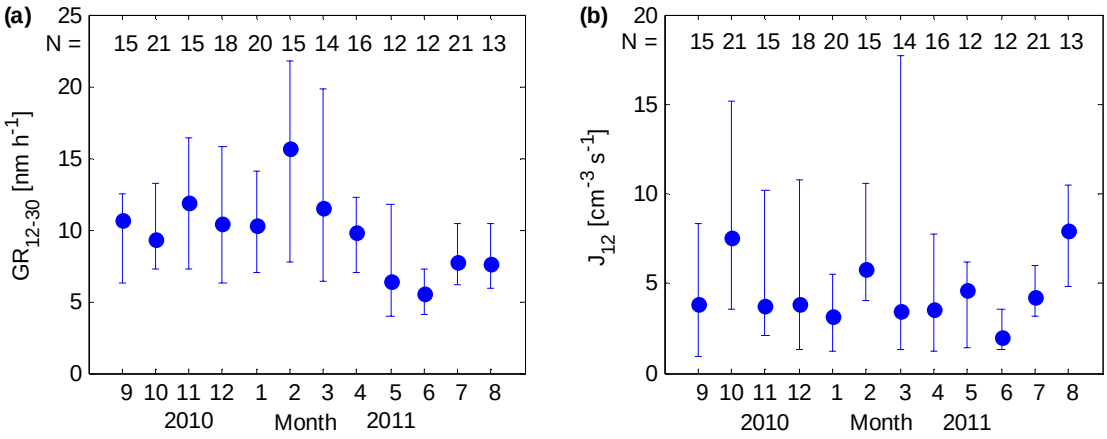

Figure S2. Monthly median $GR_{12\text{-}30}$ (**a**) and J_{12} (**b**). Error bars indicate upper and lower quartiles. Also the number of determined $GR_{12\text{-}30}$ and J_{12} is shown for each month.

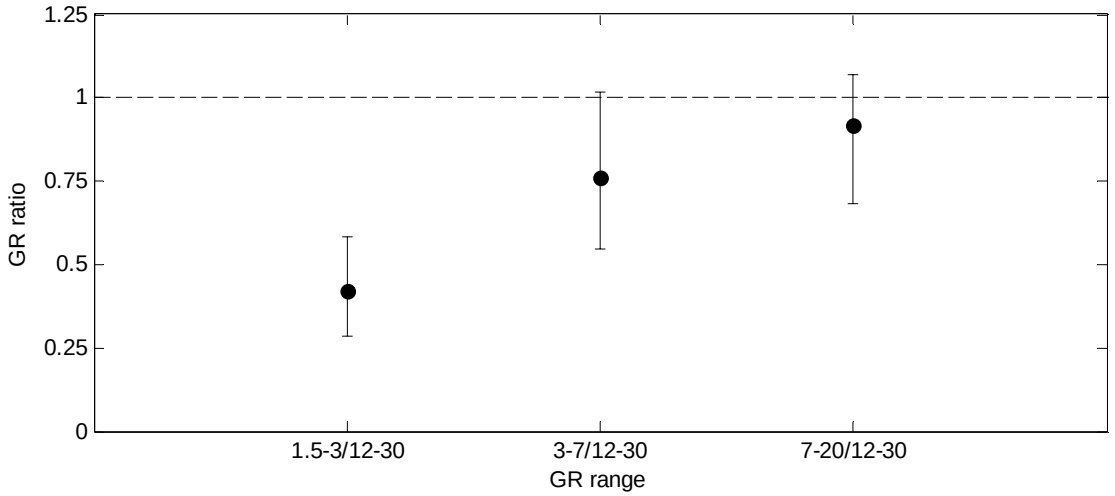

Figure S3. The median ratio of $GR_{1.5\text{-}3}$ to $GR_{12\text{-}30}$, $GR_{3\text{-}7}$ to $GR_{12\text{-}30}$ and $GR_{7\text{-}20}$ to $GR_{12\text{-}30}$. The error bars indicate upper and lower quartiles.

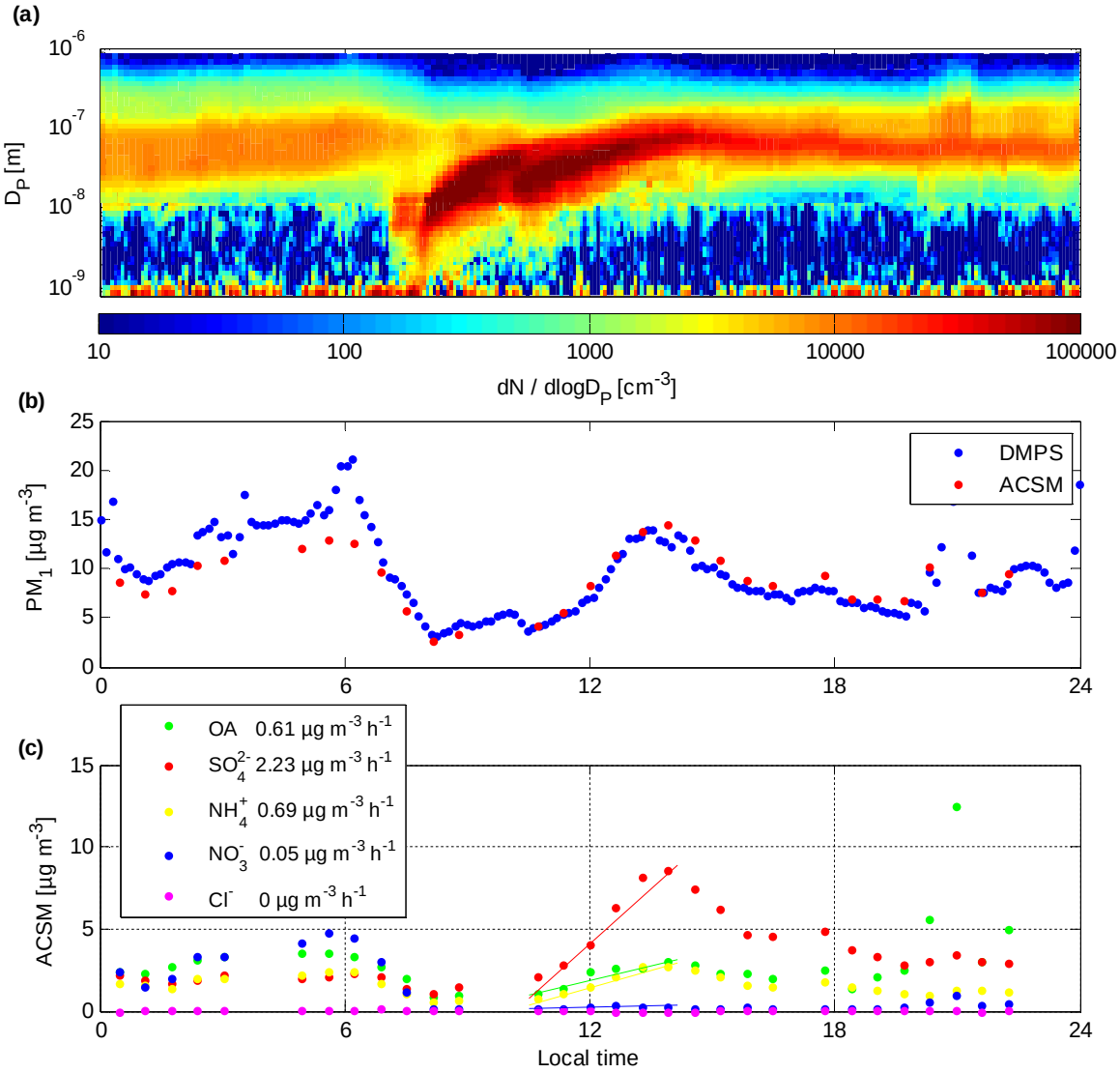

Figure S4. Measurements for 20 December 2010. **(a)** Diurnal evolution of the aerosol particle size distribution. The 12 to 840 nm size distribution is from DMPS, i.e. the sum of charged and neutral particles. Below 12 nm the size distribution is the negative polarity ion size distribution from AIS, multiplied by 30 for easier viewing. **(b)** PM_1 mass concentration estimated from the ACSM (the sum of the species characterized by ACSM) and from the DMPS size distribution using the ACSM composition information to estimate the density assuming densities of 1.3 g cm^{-3} for OA and 1.8 g cm^{-3} for inorganic compounds. **(c)** ACSM mass increase rate is obtained from a linear fit to each component separately. For this day (the second event with $GR_{12\text{-}30}$ 18.5 nm h^{-1}) Q_{ACSM} is 3.6 µg m^{-3} h^{-1}, $Q_{GR12\text{-}30}$ is 3.6 µg m^{-3} h^{-1} and Q_{J12} is 0.2 µg m^{-3} h^{-1}. Time is local time (UTC+2).

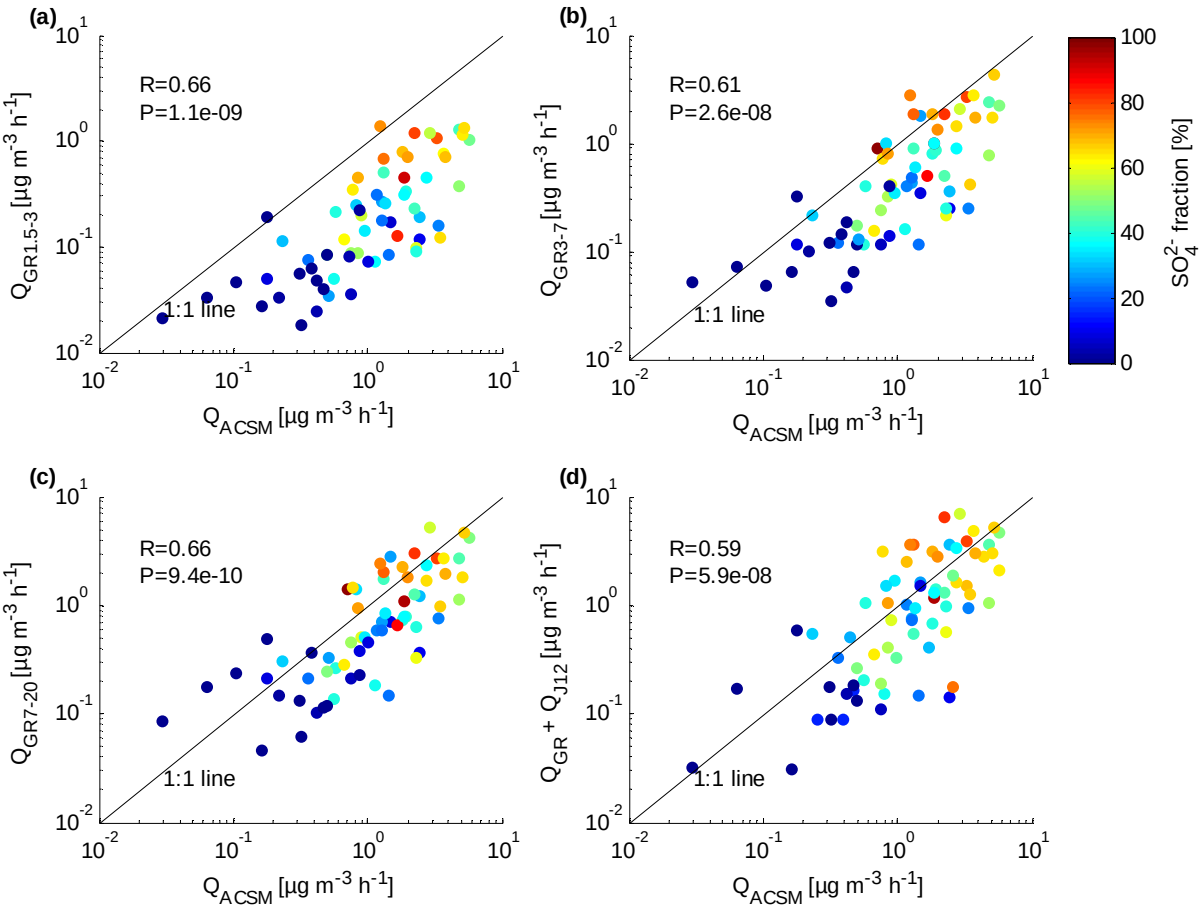

Figure S5. Observed Q_{ACSM} and Q_{GR} for four different GR size ranges. **(a)** $Q_{GR1.5-3}$ vs. Q_{ACSM}. **(b)** Q_{GR3-7} vs. Q_{ACSM}. **(c)** Q_{GR7-20} vs. Q_{ACSM}. **(d)** The sum of $Q_{GR12-30}$ and Q_{J12} vs. Q_{ACSM}. In a–c the GR is calculated as the mean of GRs calculated separately for positive and negative ions. The color indicates the fraction of SO_4^{2-} in the condensable vapors.

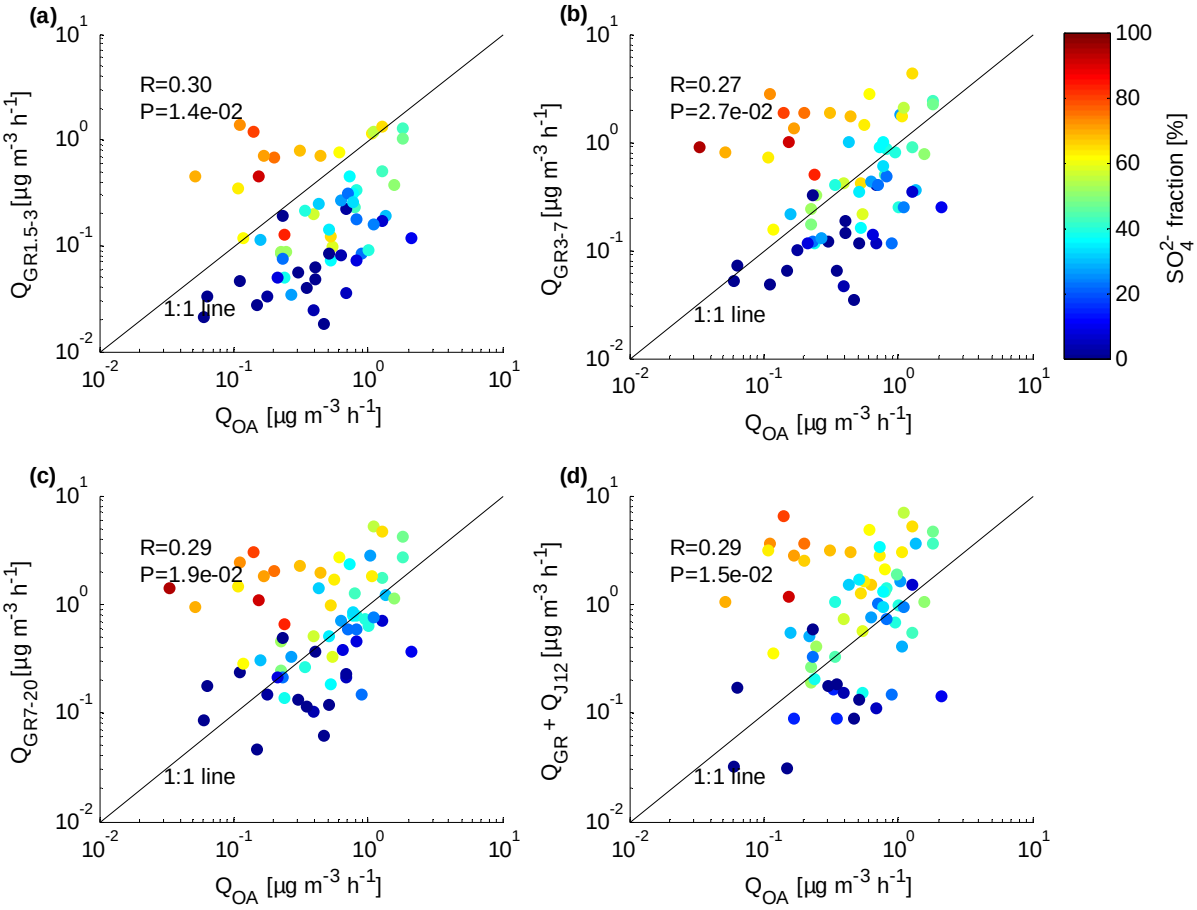

Figure S6. Observed Q_{OA} and Q_{GR} for four different GR size ranges. **(a)** $Q_{GR1.5-3}$ vs. Q_{OA}. **(b)** Q_{GR3-7} vs. Q_{OA}. **(c)** Q_{GR7-20} vs. Q_{OA}. **(d)** The sum of $Q_{GR12-30}$ and Q_{J12} vs. Q_{OA}. In A–C the GR is calculated as the mean of GRs calculated separately for positive and negative ions. The color indicates the fraction of SO_4^{2-} in the condensable vapors.

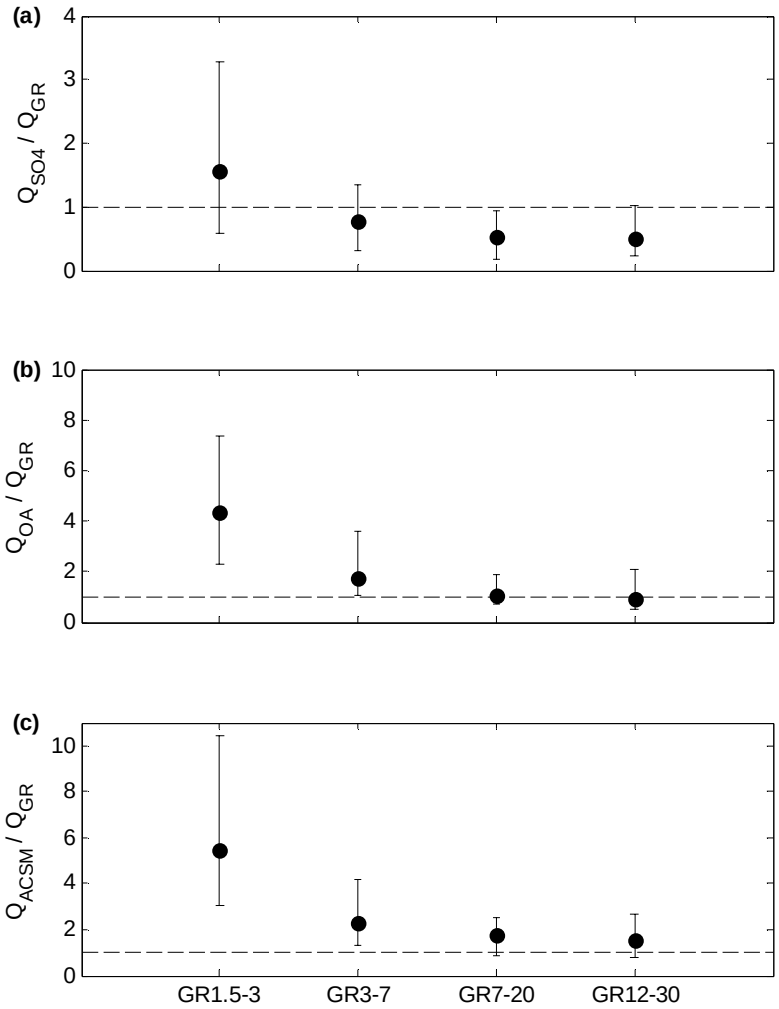

Figure S7. (a) The median ratio of Q_{SO4} to Q_{GR} for four GR size ranges. **(b)** The median ratio of Q_{OA} to Q_{GR} for four GR size ranges. **(c)** The median ratio of Q_{ACSM} to Q_{GR} for four GR size ranges. In all panels the error bars indicate upper and lower quartiles and the dashed line indicates unity.

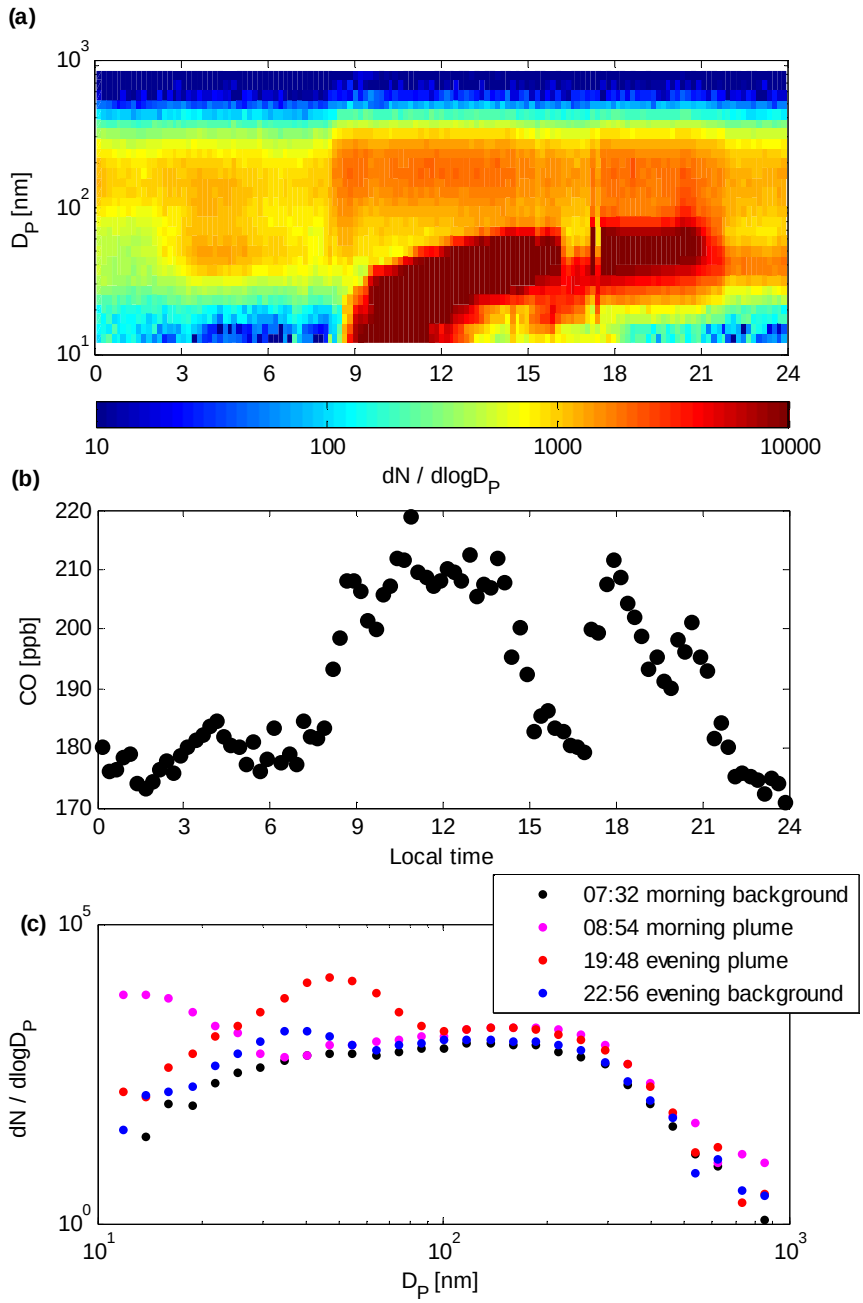

Figure S8. (a) DMPS size distribution for 4 October 2007 at Botsalano [*Laakso et al.*, 2008; *Vakkari et al.*, 2011]. **(b)** Carbon monoxide concentration on 4 October 2007 at Botsalano. **(c)** Selected size distributions inside and outside of the biomass burning plume on 4 October 2007. The effect of enhanced growth due to biomass burning is evident in the Aitken mode in the evening: out of plume peak is at 35 nm, within plume peak is at 50 nm.

Location and time	Site description	Measurements	Number of NPF events	Mass fractions [%]				Reference
				OA	SO_4^{2-}	NH_4^+	NO_3^-	
Welgegund South Africa, 26.57°S 26.94°E 1480 m a.s.l., 1 September 2010 to 15 August 2011	background grassland, impacted by urban outflow	ACSM and DMPS	88	**46**	**39**	**13**	**2**	This study
				48	38	11	3	
	Highveld (urban outflow)		17	**20**	**62**	**15**	**2**	
				26	58	14	2	
	regional background		14	**50**	**35**	**9**	**2**	
				47	41	9	2	
	clean sector		9	**87**	**3**	**0**	**2**	
				89	3	3	5	
Pittsburgh USA, 40.45°N 79.95°W, 7 to 22 September 2002	Urban	AMS and SMPS	3	**23**	**45**	**21**	**2**	Zhang et al. [2004]
				28	47	22	2	
Beijing China, 39.51°N 116.31°E, 23 August 2006	Urban	AMS and SMPS	1	SO_4^{2-} dominated				Wiedensohler et al. [2009][b]
Beijing China, 39.95°N 116.32°E, 5 June to 22 September 2008	Urban	AMS and SMPS	21	**48**	**38**	-	-	Zhang et al. [2011b][a]
				54	33			
Bakersfield USA, 35.35°N 118.97°W, 15 May to 29 June 2010	urban	AMS and SMPS	39	77	16	5	2	Ahlm et al. [2012]
Wilmington USA 39.74°N 75.56°W, 1 July 2009 to 15 July 2009	urban	NAMS and SMPS	4	**29**	**43**	**11**	**8**	Bzdek et al. [2012]
				30	43	11	8	
Brisbane Australia, 1 November to 7 December 2012	urban	AMS and NAIS	20	SO_4^{2-} and NH_4^+ dominated				Crilley et al. [2014][b]

Tecamac Mexico, 19.70°N 98.98°W 2273 m a.s.l., 16 March 2006	rural impacted by urban outflow 40 km NE of central Mexico City	SMPS and CIMS	1	84	10	-	6	Smith et al. [2008]
Lewes USA, 38.78°N 75.16°W, 15 October to 12 November 2007	background coastal impacted by coal-fired power plant 23 km away	NAMS and SMPS	7	**24** 24	**32** 33	**13** 13	**26** 24	Bzdek et al. [2012]
Lewes USA, 38.78°N 75.16°W, 23 July to 31 August 2012	background coastal impacted by coal-fired power plant 23 km away	NAMS and SMPS	2	51	27	10	10	Bzdek et al. [2013]
Lewes USA, 38.78°N 75.16°W, 23 July to 31 August 2012	background coastal impacted by coal-fired power plant 23 km away	NAMS and SMPS	4	**62** 64	**28** 26	**7** 7	-	Bzdek et al. [2014][c]
Cool USA, 38.52°N 121.01°W 450 m a.s.l., 2 to 27 June 2010	background impacted by urban outflow 40km from Sacramento	AMS and SMPS	17	**83** 84	**13** 11	-	-	Setyan et al. [2014][a]
	urban outflow		14	**78** 81	**16** 14	-	-	
	clean sector		3	**100** 100	**0** 0	-	-	
Hyytiälä Finland, 61.85°N 24.29°E 180m a.s.l., 28 March to 1 April 2003	background boreal forest	AMS and DMPS	1	100	0	-	-	Allan et al. [2006]
Hyytiälä Finland, 61.85°N 24.29°E 180m a.s.l., 9 to 17 April 2007	background boreal forest	AMS and DMPS	7	**57** 72	**32** 20	-	-	Pierce et al. [2011][a]
Egbert Canada 44.23°N 79.78°W 251 m a.s.l., 21 to 22 May 2007	background farmland, impacted by urban outflow	AMS and SMPS	2	100	0	-	-	Pierce et al. [2011][a]
Hyytiälä Finland, 61.85°N	background boreal forest	AMS, DMPS	1	80	10	5	5	Riipinen et al.

24.29°E 180m a.s.l., 23 July 2010		and NAIS						[2012]
Whistler Mountain Canada, 50.06°N 122.96°W two sites at 1300 and 2182 m a.s.l., 5 to 9 July 2010	background boreal forest	AMS and SMPS	sum of 5 consecutive events	98	0	0	2	Pierce et al. [2012]
Hyytiälä Finland, 61.85°N 24.29°E 180m a.s.l., 28 March to 19 April 2011	background boreal forest	NAMS and DMPS	8	**54** 49	**37** 40	**9** 10	-	Pennington et al. [2013]
Wakayama Japan, 34.07°N 135.52°E 750 m a.s.l., 20 to 30 August 2010	background coniferous forest	AMS and SMPS	4	OA dominated				Han et al. [2014][b]

Table S1. An overview of studies that report chemical composition of the growth in atmospheric NPF events. Measurements: aerosol chemical speciation monitor (ACSM), aerosol mass spectrometer (AMS), nano aerosol mass spectrometer (NAMS), chemical ionization mass spectrometer (CIMS), differential mobility particle sizer (DMPS) and scanning mobility particle sizer (SMPS). Both mean and median mass fractions are reported when available; median mass fractions are indicated in **bold**.

[a]Only OA and SO_4^{2-} reported, readings given assuming that SO_4^{2-} is fully neutralized by NH_4^+.

[b]Non-quantitative.

[c]Re-analysis from Bzdek et al. [2013]. 3% (both mean and median) attributed to SiO_2.

GR range [nm]	A [h molecules cm^{-3} nm^{-1}]
1.5 – 3	1.58×10^7
3 – 7	1.99×10^7
7 – 20	2.28×10^7
12 – 30	2.34×10^7

Table S2. Coefficient *A* in Eq. S1 for different GR ranges [*Nieminen et al.*, 2010].

Region	Criteria
Clean	> 20 h over clean sector, < 4 h over north-eastern sector, 0 h over Highveld
Regional background	< 5 h over clean sector, > 10 h over north-eastern sector, 0 h over Highveld
Highveld	<5 h over clean sector, > 25 h over Highveld

Table S3. Criteria for identifying NPF events representative of each source region (cf. Fig. 3).